8

Infrared Thermo-Electric Photodetectors

W. Vandermeiren[1], J. Stiens[1], G. Shkerdin[2], V. Kotov[2],
C. De Tandt[1] and R. Vounckx[1]
[1]*Vrije Universiteit Brussel,*
[2]*Institute of Radio Engineering and Electronics of the Russian Academy of Science,*
[1]*Belgium*
[2]*Russia*

1. Introduction

During the last decade, pulsed laser radiation has gained interest by the material processing industry and the medical sector. For a growing set of applications (laser drilling, laser marking, laser surgery, semiconductor doping profiling, micro-structuring, layer deposition, etc.) it is advantageous to use pulsed laser radiation instead of continuous wave (CW) illumination as time limited exposure often results in reduced collateral damage and more precise processing (Phipps, 2007). In laser ablation for example, one aims to put an intense laser pulse on the surface of a target material in an as short time as possible. This short exposure time, which limits thermal diffusion inside the material, together with a carefully selected wavelength with a minimal absorption depth is required to ensure energy deposition in a small volume of the target material. Hence, for laser pulses which meet the ablation requirements, one can evaporate material in a very controlled fashion. Different methods exists as Q-switching, mode-locking and cavity dumping for achieving the required pulse characteristics for laser ablation.

Laser pulses span an enormously large parameter space in terms of wavelength, repetition rate, pulse duration and pulse energy, further referenced as pulse-parameters. Each of these pulse-parameters can be optimized for a given application and target material. Besides its dependence on the temporal characteristics of pulsed laser radiation, for some applications, the processing quality is also strongly dependent on the transverse laser beam profile. Consequently, there is a growing interest in detecting the spatio-temporal behavior of laser pulses.

In this chapter we briefly describe the most common infrared detector principles for measuring laser pulses and point out their respective advantages and disadvantages with respect to different pulse-parameters. Next, we show that Seebeck-effect based thermo-electric photodetectors can be designed to cover a relatively broad range of pulse-parameters (Stiens, 2006). Further, we discuss the working principle and operation regimes of the thermo-electric photo detector and explain the corresponding theoretical background in detail. Experimental results concerning short laser pulse induced thermo-voltages in n-GaAs are presented. This chapter is also concerned with the possibility of using the thermo-electric effect to measure the spatio-temporal behavior of laser pulses by means of linear focal plane arrays (LFPA). Certain related issues will be highlighted such as

thermal cross-talk between pixels in case of pulse durations approaching CW illumination. A lock-in method is proposed to reduce the cross-talk level. The chapter will conclude with describing the future directions of research.

2. Infrared detector principles

This section deals with the most common infrared detector principles based on various physical mechanisms and materials for measuring laser pulses. Interest is mainly focused on wavelengths of the two atmospheric windows 3–5 μm (middle wavelength IR - MWIR) and 8–14 μm (low wavelength IR- LWIR) as in these bands the atmospheric transmission is highest, though in recent years, there has been increasing interest in longer wavelengths stimulated by space applications. Figure 1 (Rogalski, 2003)[1] shows the spectral detectivity curves for a number of commercially available IR detectors.

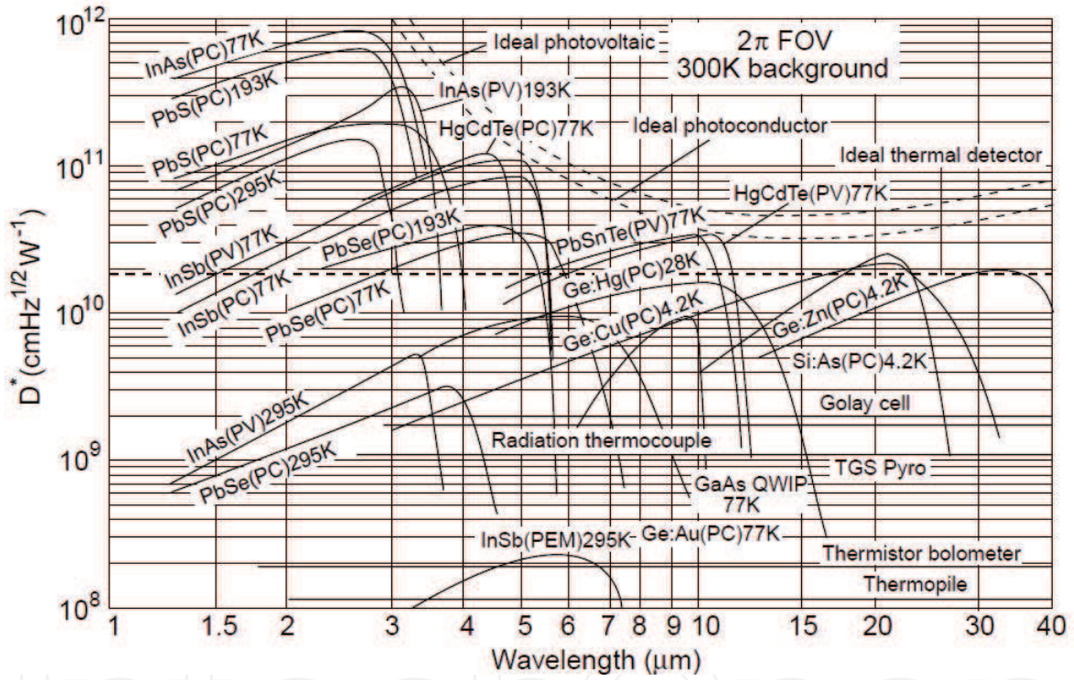

Fig. 1. Comparison of the detectivity D* of various commercially available infrared detectors when operated at the indicated temperature. Chopping frequency is 1000 Hz for all detectors except for the thermopile, thermocouple, thermistor bolometer, Golay cell and pyroelectric detector, where it is 10 Hz. Each detector is assumed to view a hemispherical surrounding at a temperature of 300 K. Theoretical curves for the background-limited D*(dashed lines) for ideal photovoltaic and photoconductive detectors and thermal detectors are also shown. PC—photoconductive detector, PV—photovoltaic detector, and PEM—photoelectromagnetic detector.

The main specifications that one has to consider while comparing different detector principles and materials are next to the spectral detectivity, the response speed, whether

[1] Reprinted from Progress in Quantum Electronics, Vol.27/2-3, Infrared detectors: status and trends, pp. 59-210, Copyright 2003, with permission from Elsevier.

cryogenic operation temperatures are required and the damage threshold. The relative importance of each of these detector parameters is typically strongly related to the application. In case of low power laser pulses, a high responsivity is of major importance while for measuring industrial high power laser pulses, a lower responsivity might be desirable as for most IR detectors, the power handling capability, which is limited by the maximum temperature increase on the detector surface, is inversely proportional to the absorption coefficient (see Eq. 23). Note that this is only true for short exposure times. At long exposure times, the damage threshold intensity becomes independent of the absorption coefficient.

Infrared detectors can be classified into thermal and photon detectors depending on their detection mechanism. A brief overview of IR detectors with their inherent advantages and disadvantages are classified and summarized in table 1 (Rogalski, 2003).

	Detector type	Advantages	Disadvantages
Thermal detectors	**Thermopile, bolometers, pyroelectric**	Light, rugged, reliable and low cost, room temperature operation	Low detectivity @ high frequency Slow response (ms order)
Photon detectors	**Intrinsic**		
	IV-VI	Easy to prepare	High thermal expansion coefficient
	(e.g. PbS, PbSe, PbSnTe)	More stable materials	Large permittivity
	II-VI	Easy bandgap tailoring	Non-uniformity over large area
	(e.g. HgCdTe)	High optical absorption	High cost in growth and processing
		Low thermal generation	Surface instability
	III-V	Good material and dopants	Heteroepitaxy with large lattice mismatch
	(e.g. InGaAs, InAs, InSb, InAsSb)	Advanced technology	Long wavelength cutoff limited to 7 μm
		Possible monolithic integration	
	Extrinsic		
	(e.g. Si:Ga, Si:As, Ge:Cu, Ge:Hg)	Very long wavelength operation	High thermal generation
		Simple technology	Extremely low temperature operation
	Free carriers		
	(e.g. PtSi, Pt_2Si, IrSi)	Low cost, high yield	Low quantum efficiency
		Large & close packed 2D arrays	Low temperature operation
	Quantum Wells		
	Type 1	Matured material growth	High temperature generation
	(e.g. GaAs/AlGAAs, InGaAs/AlGaAs)	Good uniformity over large area	Complicated design & growth
	Type 2	Low Auger recombination rate	Complicated design & growth
	(e.g. InAs/InGaSb, InAs/InAsSb)	Easy wavelength control	Sensitive to the interfaces
	Quantum dots		
	(e.g. InAs/GaAs, InGaAs/InGaP, Ge/Si)	Normal incidence of light	Complicated design & growth
		Low thermal generation	

Table 1. IR detector classification.

2.1 Thermal detectors

The output signal of thermal detectors is observed as a temperature dependent property change in the active detector material. This temperature dependent mechanism can result in

a thermoelectric voltage, a resistance change or a pyroelectric voltage depending on the detector type. Table 2 shows different thermal detectors with the corresponding temperature dependency of the detector's output. Thermal detectors are often characterized by a relatively slow response time and low detectivity, which make them less suitable for short and low intensity optical pulses. Their photo sensitivity is typically independent on the wavelength as a broad band absorption layer is used as a window material to convert the optical intensity into heat. In contrast with most photon detectors, they can operate at room temperature. Forced cooling is only required for detectors which are designed for high average optical power levels.

Detector type	Signal (T)
Thermocouple	~ΔT
Bolometer	~T
Pyroelectric	~ dT/dt
Forward-bias diode	~T

Table 2. Different types of thermal detectors

Assuming a periodic optical radiation, the temperature change in a thermal based IR is given by:

$$\Delta T = \frac{\varepsilon\Phi_0}{(G_{th}^2 + \omega^2 C_{th}^2)^{1/2}} = \frac{\varepsilon\Phi_0 \mathrm{R_{th}}}{(1+\omega^2\tau_{th}^2)^{1/2}} \qquad \text{with} \qquad \tau_{th} = \frac{C_{th}}{G_{th}} = \mathrm{R_{th}C_{th}} \tag{1}$$

Where ε, Φ_0, R_{th}, ω, C_{th}, τ_{th} are the absoptivity, the incident radiative flux, the thermal resistivity, the angular frequency, the thermal capacitance and the thermal response time constant, respectively. In order to make ΔT as large as possible, one should use a detector material with a small thermal conductivity and a small thermal capacitance. The thermal response time is typically of the order of milliseconds. Hence, thermal detectors are less suitable for high speed measurements.

The voltage responsivity (R_v) is then defined as the ratio of the detector output signal to the input radiation power

$$R_v = \frac{\Delta V}{\Phi_0} = \frac{\Delta V}{\Phi_0 \Delta \mathrm{T}} \frac{\varepsilon\Phi_0 \mathrm{R_{th}}}{(1+\omega^2\tau_{th}^2)^{1/2}} = \frac{K\varepsilon \mathrm{R_{th}}}{(1+\omega^2\tau_{th}^2)^{1/2}} \quad \text{with} \quad K = \frac{\Delta V}{\Delta \mathrm{T}} \tag{2}$$

The well-known detectivity criteria D* is widely used for comparing detectors, as D* is independent on the size and shape of the detector. The detectivity of thermal detectors can be calculated when the noise mechanisms are known. Hence, D* is a measure of the signal-to-noise (S/N) ratio of the detector. The main noise mechanism consists of Johnson noise. This noise in a Δf bandwidth for a resistor R is given by expression (3) where k_B and T are the Bolzmann constant and the temperature, respectively.

$$V_J^2 = 4k_B T R \Delta f \tag{3}$$

In addition to Johnson noise, other noise sources which contribute to the overall noise level are 1/f noise, thermal fluctuation noise and background noise. The thermal fluctuation noise and background noise can be shown to be (Rogalski, 2003)

$$V_{TF}^2 = \frac{4k_B T^2 \Delta f}{1+\omega^2\tau_{th}^2} K^2 R_{th} \qquad V_B^2 = \frac{8k_B \varepsilon\sigma A(T_d^2 + T_b^2)}{1+\omega^2\tau_{th}^2} K^2 R_{th} \tag{4}$$

Where σ is the Stefmann-Boltzmann constant. Hence, the detectivity D* of a thermal fluctuation noise limited and background fluctuation noise limited detector are given by expressions(5ab) (Rogalski, 2003), respectively, where A_d is the detector surface.

$$D_{TF}^* = \frac{(A_d \Delta f)^{1/2}}{V_{TF}} R_v = \left(\frac{A_d \varepsilon^2 R_{th}}{4k_B T^2} \right)^{1/2} \qquad D_B^* = \left(\frac{\varepsilon}{8k_B \sigma (T_d^5 + T_b^5)} \right)^{1/2} \tag{5}$$

Typical detectivities of thermal detectors (at 10Hz) are of the order of 10^8 - 10^9 cmHz$^{1/2}$W^{-1}.

2.2 Photon detectors

Photon detectors (e.g. photoconductive, photovoltaic, photo-electromagnetic detectors) absorb the radiation within the active material due to electron-hole creation. The observed electrical output signal is the consequence of a changed electronic energy distribution. In contrast with thermal detectors, photon detectors offer a higher detection performance and a faster response speed, although their photosensitivity is strongly wavelength dependent and most of them are cryogenically cooled for optimal performance in terms of sensitivity and signal-to-noise ratio.

The current responsivity R_i of photon detectors is proportional to the photoelectric gain (g) and the quantum efficiency (η). The quantum efficiency is a measure for the device's electrical sensitivity to light and is usually defined as the percentage of photons incident in the active area of the detector that produce an electron-hole pair. The photo-electric gain is the number of carriers collected at the contacts per generated pair. Hence the current responsivity equals

$$R_i = \frac{\lambda\eta}{\mathrm{hc}} qg \tag{6}$$

Where λ is the wavelength, h is the Planck's constant, c is the light velocity and q is the elementary charge. The current noise associated to the generation and recombination can be defined as follows

$$I_n^2 = 2(G+R) A_e t \Delta f q^2 g^2 \tag{7}$$

Where G and R are the generation and recombination rates, Δf is the frequency band, A_e is the electrical area and t is the thickness of the detector. The detectivity can then be defined as

$$D^* = \frac{R_i (A_o \Delta f)^{1/2}}{I_n} = \frac{\lambda}{\mathrm{hc}} \left(\frac{A_o}{A_e} \right)^{1/2} \frac{\eta}{(2(G+R)t)^{1/2}} \tag{8}$$

Where A_o is the optical surface. Assuming a single pass of the radiation and consider $A_o = A_e$, the expression for D* simplifies to

$$D^* = \frac{R_i (A_o \Delta f)^{1/2}}{I_n} = \frac{\lambda}{\mathrm{hc}} \frac{\eta}{(2(G+R)t)^{1/2}} \quad \text{with} \quad \eta = 1 - e^{-\alpha t} \tag{9}$$

Where α is the wavelength dependent absorption coefficient for a material under consideration. One can easily derive that a maximum detectivity is achieved for t = 1.26/α. In order to achieve an optimal detectivity, thermal generation should be reduced as much as possible. This is usually done with cryogenic cooling of the detector. Figure 1 shows that detectivities of photon detectors are of the order of 10^9 – 10^{11} $cmHz^{1/2}W^{-1}$, which is typically 1 to 2 orders of magnitude higher as compared to thermal detectors.

2.3 Comparison

Within the category of photon detectors, one sees that the performance of intrinsic IR detectors (e.g. HgCdTe), in terms of detectivity, is higher than other types of photon detectors. HgCdTe is characterized by a high optical absorption coefficient and quantum efficiency and relatively low thermal generation rate compared to extrinsic detectors and quantum well infrared photodetectors (QWIPs). The extrinsic photon detectors require more cooling than intrinsic photon detectors having the same long wavelength limit.

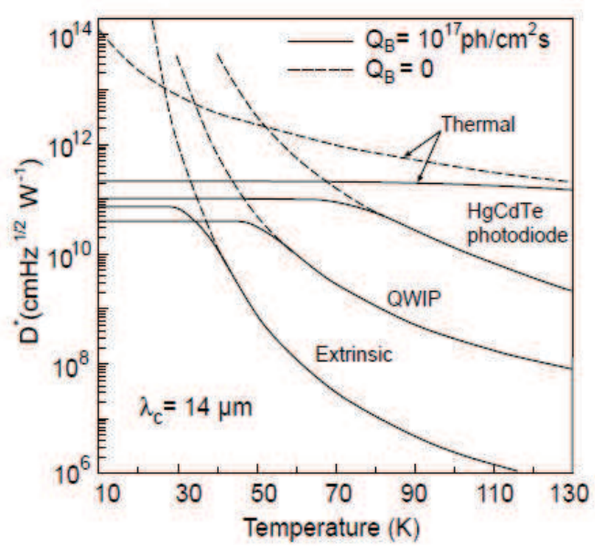

Fig. 2. Theoretical detectivity limits of LWIR photon and thermal detectors at a wavelength of 14 μm as a function of the detector temperature for zero background and a background of 10^{17} photons $cm^{-2}s^{-1}$.

One can deduce from figure 1 and 2 (Rogalski, 2003)[2] that the detectivity of thermal detectors is less temperature and wavelength dependent as compared to photon detectors. At temperatures below 50 K and zero background, LWIR thermal detectors are characterized by a theoretical performance limit (D*) lower than those of LWIR photon detectors. However, at temperatures above 60 K, the thermal detectors outperforms the LWIR photon detectors. At room temperature, the theoretical performance of thermal detectors is much better than LWIR photon detectors. The comparison of both types of detectors indicates that theoretical performance limits for thermal detectors are more favorable as wavelength of operation moves from the LWIR to the VLWIR.

[2] Reprinted from Progress in Quantum Electronics, Vol.27/2-3, Infrared detectors: status and trends, pp. 59-210, Copyright 2003, with permission from Elsevier.

Thermal detectors have a low time response of the order of milliseconds, limited by the thermal time constant of the detector. This property makes them less suitable for short pulse measurements. Intrinsic photon detectors on the contrary have a time response which is at least three orders of magnitude faster than for thermal detectors.

3. Seebeck infrared photodetector

A Seebeck infrared photodetector can be categorized as a special kind of thermal detector which can be operated at room temperature. The operation principle of this detector type is based on photon induced free carrier absorption in doped semiconductors. Detailed calculations have been performed for n-GaAs. The material choice is based on the performance and price level of n-GaAs with respect to other materials. The optical intensity decays exponentially along the axis of propagation inside the highly doped region of the semiconductor material (e.g. n-GaAs), as a result of the absorption process. Consequently, a temperature gradient is generated. This temperature gradient leads to free carrier diffusion in the conducting layers of the structure which provokes a change in the electron concentration and creates an electrical field inside the substrate. This thermo-electric effect is characterized by a Seebeck coefficient (S) which is dependent on temperature, the doping concentration and the crystal structure of the semiconductor material. The detector output is then given by:

$$V_{out} = S \cdot \Delta T_e \tag{10}$$

Where ΔT_e is the temperature difference between two electrodes on the substrate. Note that here, unlike most other thermal detectors, the absorbing window material and the active detector material are the same. Hence, the spectral window of semiconductor based Seebeck detectors is dependent on the spectral free carrier absorption process.

3.1 Seebeck coefficient

To calculate the Seebeck coefficient, one has to solve the kinetic equation for the electron distribution function in the presence of an electron temperature gradient. Taking into account the nonparabolicity of the Γ-valley and the anisotropy of the satellite L- and X-valleys of n-GaAs, the expression for S can be written as follows:

$$S = \frac{k_B(a_\Gamma\sigma_\Gamma + a_L\sigma_L + a_x\sigma_x)}{(\sigma_\Gamma \cdot \sigma_L \cdot \sigma_x)} \tag{11}$$

Where k_B and q are the Boltzmann constant and the elementary charge, respectively; $\sigma_{\Gamma,L,X}$ and $a_{\Gamma,L,X}$ are the electron conductivity and the dimensionless weighting coefficients for the Γ, L and X valley, accordingly. The contribution of the phonon-drag effect to the thermo-electric power is neglected as the active semiconductor layer is degenerate and the operation temperature is relatively high T ≥ 297 K (George et al., 2001). The contributions of the satellite valleys are small near room temperature for doping concentrations $n_0 \leq 7x10^{18}$ cm^{-3}. In this case the expression for S simplifies to:

$$S \approx \frac{k_B}{q} a_\Gamma \tag{12}$$

Where a_Γ is a dimensionless weighting factor which can be calculated as follows:

$$a_\Gamma = \frac{1}{k_B T_e}\left(-\xi + \frac{\int_0^\infty d\varepsilon_\Gamma (\varepsilon_\Gamma{}^2 + \gamma\varepsilon_\Gamma{}^3/E_g)^{3/2}(1+2\gamma\varepsilon_\Gamma/E_g)^{-1}\tau_\Gamma f'_{o,\Gamma}}{\int_0^\infty d\varepsilon_\Gamma (\varepsilon_\Gamma + \gamma\varepsilon_\Gamma{}^2/E_g)^{3/2}(1+2\gamma\varepsilon_\Gamma/E_g)^{-1}\tau_\Gamma f'_{o,\Gamma}} \right) \tag{13}$$

where τ_Γ is the momentum relaxation time in the Γ-valley; $f'_{0,\Gamma} = df_0/d\varepsilon_\Gamma$ where f_0 is the 0^{th} order Fermi-Dirac distribution function. T_e, E_g, γ, ε_Γ are the electron temperature, bandgap, band non-parabolicity factor and electron energy in the Γ-valley, respectively. The electron spectrum of the Γ-valley can be approximated by:

$$\varepsilon_\Gamma = \frac{E_g}{2\gamma}\left(\sqrt{1 + \frac{2\gamma}{E_g}\frac{\hbar^2\vec{k}^2}{m_\Gamma}} - 1 \right) \tag{14}$$

Where ε_Γ is the electron energy counted from the bottom of the Γ-valley, k is the electron wave vector, m_Γ is the electron effective mass at the bottom of the Γ-valley.

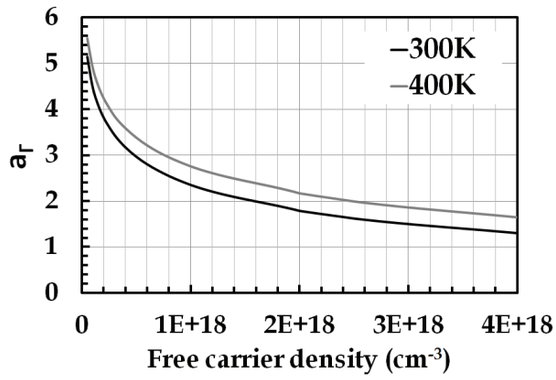

Fig. 3. Dependences of a_Γ on thefree electron density for two temperatures T_e = 300 K and 400 K (n-GaAs)

Dependences of a_Γ versus doping concentration for two temperatures T_e = 300 K and 400 K are shown in figure 3. Notice that a_Γ is positive and of the order of one which corresponds to a Seebeck coefficient of the order of 100 μV/K. Hence, the voltage responsivity of a n-GaAs based Seebeck detector, which can be calculated by means of Eq. 2, is of the order of a few mVW^{-1}. A logarithmic fit on these data at room temperature results in the following approximation for the Seebeck coefficient for $1x10^{17} < n_0 < 4x10^{18}$:

$$S \approx -72.9 \ln\left(\frac{n_0}{10^{18}}\right) + 207.4 \quad \left(\frac{\mu V}{K}\right) \tag{15}$$

One can also see that an increase of the electron gas degeneracy leads to a decrease of the Seebeck coefficient and an increase of the electrical conductivity. It is important to mention that the electrical conductivity should be high enough to probe the thermo-electromotive force (emf) induced potential. Therefore, a typical figure of merit for thermo-electric devices is given by:

$$Z = \frac{S^2\sigma}{k_{th}} \tag{16}$$

Where, σ and k_{th} are the electrical and thermal conductivity, respectively. As the contributions of conduction carriers to the thermal conductivity are in general very small (Sze, 1981), Z (~$S^2\sigma$) will be maximal for a given doping concentration.

3.2 Thermo-voltage detector - detectivity

However, in order to maximize the detectivity of Seebeck based detectors, one should take into account the free electron absorption coefficient for the wavelength under consideration, which is strongly dependent on the doping concentration. Calculations were performed based on an multi-valley (Γ, X, L) model where non-parabolic and anisotropic effects are taken into account for the intravalley and (non)equivalent intervalley absorption mechanisms (Shkerdinet al., 1999). The absorption coefficient was calculated for wavelengths between 8 μm < λ < 19 μm and an electron density between 10^{17} cm^{-3} < n_0 < 10^{18} cm^{-3}. A compensation factor, given by Eq. 17,equal to one is assumed such that the contribution of impurity scattering on compensated donor and acceptor atoms to the absorption coefficient is neglected.

$$F_{comp} = \frac{N_D + N_A}{N_D - N_A} \tag{17}$$

Here, N_D and N_A are the donor and acceptor concentration, respectively. Figure 4 shows the absorption coefficient dependency on wavelength and electron density for n-GaAs. Note that the quantum mechanical model (Shkerdin et al., 1999), comprising a compensation factor dependent absorption coefficient, allows a good agreement with experimental data. However, no direct agreement can be found with experimental data from literature, e.g. (Blakemore, 1982), when no information is available about the compensation factor.

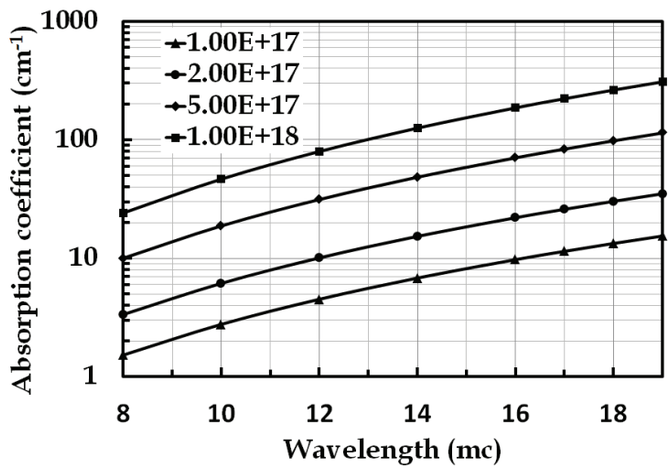

Fig. 4. Absorption coefficient dependence on wavelength and electron density for n-GaAs

Seebeck detectors can be categorized as thermal detectors. Assuming that only Johnson noise is present, we obtain:

$$D_J^* = \frac{(A_o \Delta f)^{1/2}}{V_J} R_v = S\varepsilon \mathrm{R_{th}} \left(\frac{A_d}{4k_B TR(1+\omega^2 \tau_{th}^2)} \right)^{1/2} \tag{18}$$

Where S is the Seebeck Coefficient. For a single pass, the absorptivity ε is given by

$$\varepsilon = 1 - e^{-\alpha_e t} \tag{19}$$

Where t and α_e are the highly doped layer thickness and the electron absorption coefficient.

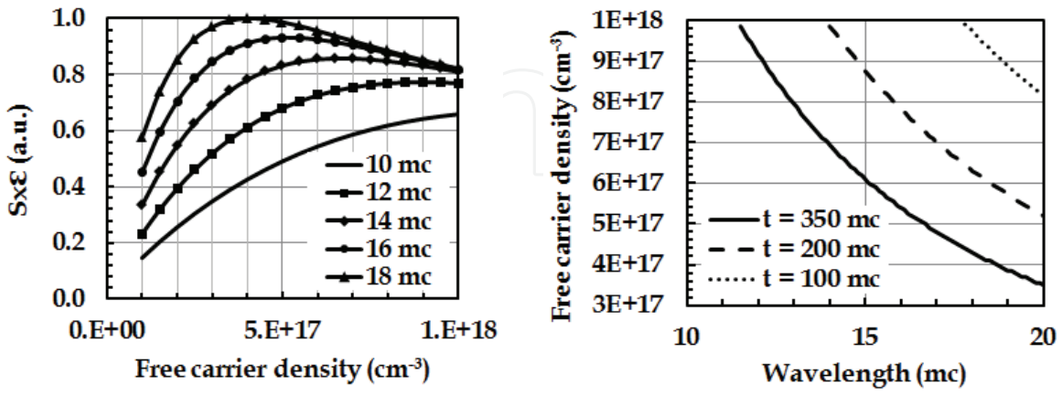

(a) (b)

Fig. 5. (a) Detectivity optima in function of the free carrier density for different wavelengths for an absorption layer thickness of 350 μm; (b) Optimal free carrier density versus wavelength for different absorption layer thicknesses

Notice that, the Seebeck coefficient (S) and the absorptivity (ε) are the only parameters in Eq. 18 which are significantly dependent on the doping concentration. The latter is also strongly dependent on the wavelength and the absorption layer thickness. Hence, the detectivity D* of a n-GaAs based Seebeck detector can be optimized for a given wavelength and absorption layer thickness by tuning the doping concentration as illustrated in figure 5a and figure 5b. These detectivity maxima shift to lower doping levels as the $\alpha_e t$ product increases. The absorption coefficient was calculated in according with a multi-valley model (Shkerdin et al., 1999). As compared to measured absorption coefficients (Blakemore, 1982), which are slightly higher as explained above, the optimal detectivity will shift to lower carrier densities with Δn_o of the order of 0.5×10^{18} cm^{-3}. Notice that the doping level is generally not critical as these optima are relatively wide. Figure 5b shows the optimal free carrier concentration in n-GaAs versus wavelength for various absorption layer thicknesses. It indicates that for relatively small wavelengths (e.g. 10.6 μm) in combination with modest absorption layer thicknesses (t < 100 μm), high optimal doping levels are found. High doping levels, however (e.g. $N_{D,GaAs} > 4 \times 10^{18}$ cm^{-3}), are technologically difficult to realize in III-V semiconductors due to self-compensation. Although, it can be accomplished by the use of special growth techniques as "Delta-doping" (Schubert, 1996).

3.3 Operation regimes

The type of detector output, and consequently the information that can be obtained, is determined by the ratio between the laser pulse duration and various time constants of the detector. The operation regimes and most important time constants which define the operation regime transitions are schematically illustrated in figure 6.

The following time constants are important: the electron heating time, the electron energy relaxation time τ_e and the lattice thermal response time τ_{ia}. The relaxation time of optically heated electrons which is dependent on the doping concentration and the incident light

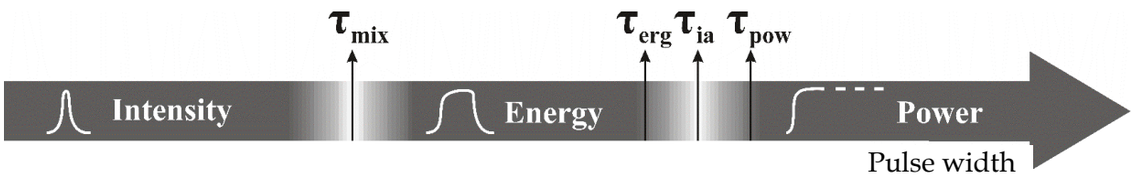

Fig. 6. Operation regimes of a semiconductor based thermo-eletric detector

intensity is of the order of a few picoseconds. For example, the relaxation time of longitudinal-optical phonon thermalization is about 3-7 picoseconds (Shah et al., 1970) (Vaissiere et al., 1992) Hence, for short incident laser pulses which are longer than a few electron energy relaxation time constants, the detector's voltage output will be proportional to the temporal evolution of the laser intensity. This "intensity"-regime is characterized by a high damage threshold of the order of 0.1-1 GWcm^{-2} as the lattice temperature is almost unaffected for such short pulses. The damage threshold in terms of maximum intensity in function of the pulse full-width halve-maximum (FWHM) is illustrated in figure 10 for different detector dimensions. In this regime, the detector's output is independent on the thermal material properties as the heat capacity C_{th} and the thermal conductivity k_{th}. This regime is also characterized by a relatively low responsivity of the order of 4-8 mV/MWcm^{-2} for highly doped n-GaAs. Consequently, this regime of operation is extremely suitable for direct measurements of short laser pulses having high optical intensities. The heating of free electron gas in doped n-GaAs is described in detail in (Shkerdin et al., 2007)

For systematically increased laser pulse widths, the electron gas will gradually transfer energy to the lattice of the doped semiconductor allowing the lattice temperature to increase. The response time of this lattice heating mechanism is much slower (10-100 μs) than electron heating. The pulse length for which the electron temperature equals the lattice temperature is called τ_{mix}. This is the regime of the mixed electron-lattice effects. τ_{mix} can be expressed as (20a) for low optical intensities, where τ_{en}, $C_{th,}$ are the stationary energy relaxation time and the volumetric heat capacitance, respectively. For high optical intensities, this response time should be corrected for non-linear behavior, resulting in expression (20b)

$$\tau_{mix} = \frac{\tau_{en} C_{th}}{N k_B} \qquad \tau_{mix} = \frac{\delta T_e C_{th}}{\alpha_e W} \tag{20}$$

The dependence of τ_{mix} on electron concentration for small laser intensities was calculated using the model developed in (Shkerdin et al., 1999) (Shkerdin et al., 2002) and is illustrated in figure 7.

These numerical simulations show that within the doping concentration interval 0.7x10^{18} - 4x10^{18} cm^{-3}, the value τ_{mix} can drop from the range 325 - 40 ns down to 100 - 10 ns when the intensity varies from a low level to about 100 MWcm^{-2}. For a certain range of pulse widths longer than τ_{mix}, the lattice temperature will increase proportional to the pulse energy. However, the energy regime is limited by the thermal response time of the illuminated area (τ_{ia}). The illuminated area time constant τ_{ia} does not only depend on material parameters, but also on the pixel geometry. The thermal response time of the illuminated area is described by

$$\tau_{ia} = \frac{\beta C_{th}}{k_{th}\left(\frac{1}{L_{abs}^2} + \frac{4}{L_{illum}^2}\right)} \tag{21}$$

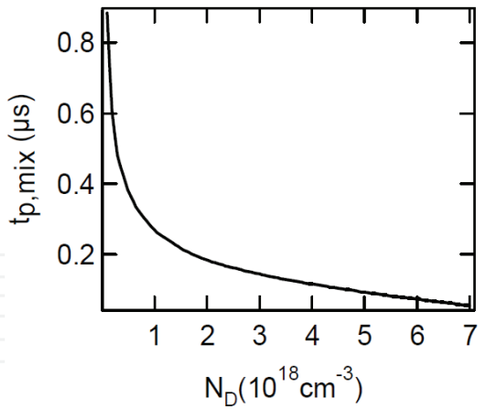

Fig. 7. Doping density dependence on τ_{mix}

Where L_{abs}, L_{illum}, are the absorption length inside the substrate and the illumination length which can be the characteristic size of a pixel or the laser beam width. β is a geometrical numerical factor of the order of one which depends on the pulse characteristics and the geometry. C_{th} and k_{th} are the volumetric heat capacitance and the thermal conductivity, respectively.

As the pulse length approaches τ_{ia}, the local lattice temperature will become less dependent on the pulse length due to thermal diffusion (lattice conductivity). Hence, for pulse lengths much larger than τ_{ia}, the lattice temperature is independent on the pulse width. This corresponds to a power measurement. The detector's maximum output can then be estimated using the following expression:

$$T_{surface,max} = \frac{W_0 L_{illum}^2}{k_{th}(L_{abs}+L_{illum})} \tag{22}$$

Where k_{th} and W_0 are the thermal conductivity and the optical intensity, respectively. In general, one can say that the power regime is characterized by a relatively high responsivity of the order of 0.01-0.1 $mVW^{-1}cm^{-2}$ for n-GaAs and a significantly lower damage threshold as compared to the intensity regime (see figure 10).

3.4 Study of a short pulse induced thermo-voltage in n-GaAs

By exposing an n-doped GaAs substrate to short optical CO_2 laser pulses with a pulse width smaller than τ_{mix}, one can distinguish the electron and lattice heating process. This section will describe the experimental setup and discuss the obtained results. The experimental setup is illustrated in figure 8.

A CO_2 laser produces short optical pulses with a pulse width of about 100 ns at a wavelength of 10.6 µm. These pulses propagate through an attenuating system consisting of two polarizers. About 50% of the power is reflected on a ZnSe beam splitter. This part is subsequently attenuated to a save intensity and measured by a reference photo electro magnetic (PEM) detector. The second part which propagates through the beam splitter is focused on a highly doped n-GaAs sample ($5x10^{17}$ cm^{-3}). This resulted in a beam width of about 170 µm on the top surface of the substrate. The incident pulse energy was limited to about 0.1 mJ to avoid non-linear thermal effects. The laser pulse induced thermo-voltage is then measured by means of a ground electrode at the backside of the substrate and a needle

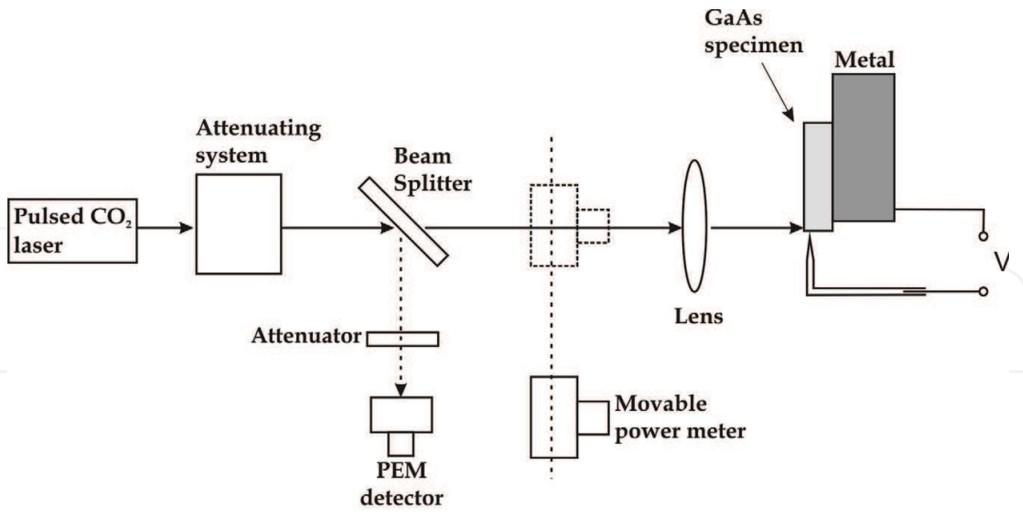

Fig. 8. Experimental setup for laser pulse induced thermo-voltage measurements

electrode positioned at about 50 μm from the top surface of the substrate. Note that the needle should be placed relatively close to the top surface of the substrate (typically smaller than the absorption length) to measure the electron heating process due to the absence of thermal diffusion in the intensity regime. The optical pulses expose the top surface of the substrate in the neighborhood of the needle. Special attention was paid to create an ohmic contact between the needle and the semiconductor material. The electrical signals of the PEM detector and the GaAs specimen are illustrated in figure 9. Here, the upper and lower curves corresponds to the laser pulse induced thermo-voltage in n-GaAs and the PEM detector output, respectively. The solid curves are experimental data, while the dashed curves corresponds to an analytical model for the laser pulse induced thermo-voltage behavior (Shkerdinet al., 2007). It was estimated that τ_{mix} is about 380 ns for a doping concentration of $5x10^{18}$ cm^{-3}. The laser pulse induced voltage consists of a first pulse which is a consequence of two mechanisms: the thermo-voltage effect due to electron gas heating and the photon drag effect. These mechanisms are fast and lead to the voltage linear temporal dependence that is proportional to the temporal intensity dependence of the incident optical pulse.

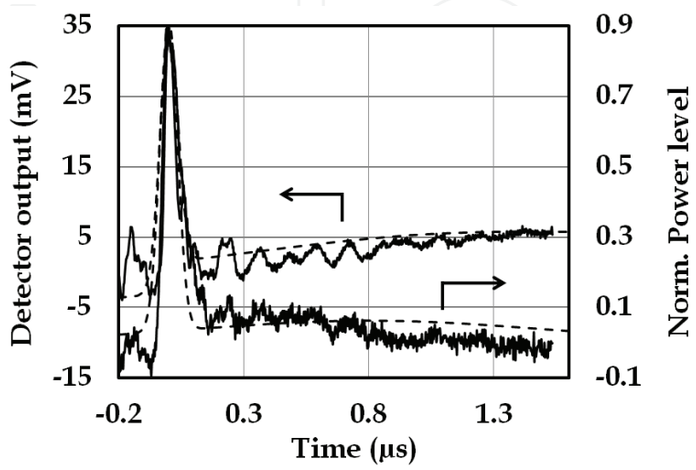

Fig. 9. Pulse induced voltage – n-GaAs versus PEM detector output

The measured combined sensitivity of the fast mechanisms is about 2.6 mVcm^2/MW, therefore these mechanisms can be useful to detect fast (sub-ns) pulses of large intensity (> 1MWcm^{-2}). The illustrated pulse is followed by a comparatively long tail which can be association to the electron-lattice interaction. The temporal voltage dependence in this region is proportional to the pulse energy temporal dependence for time duration smaller than a few microseconds when the lattice heat conduction effect is rather small. For the theoretical model describing this phenomena in detail, we refer to (Shkerdinet al., 2007)

3.5 Damage threshold

The damage threshold of a detector can be defined as the maximum intensity at which the detector may be exposed for a given exposure time and beam size. This intensity strongly depends on the wavelength dependent absorption coefficient, the beam size and the thermal parameters of the detector material. A simple analytical model can be used to estimate the energy density required to damage a particular material as reported by (Bartoli, 1977). This formula is valid for a semi-infinite solid irradiated by a Gaussian beam $P(r) = P_0 \exp(-r^2/a^2)$.

$$E_0 = \frac{\Delta T \rho c}{(1-R)\alpha_e}\left[1 + \frac{\alpha_{th}\tau\alpha_e\pi^{1/2}}{a\tan^{-1}(4k\tau/a^2)^{1/2}}\right] \tag{23}$$

Here, ΔT is the minimum increase in surface temperature at the heating centre which is required for damage, τ is the pulse width, ρ is the density, c is the specific heat, α_{th} is the thermal diffusivity, α_e is the absorption coefficient, R is the reflection coefficient and a is the beam size. Figure 10a shows the resulting damage threshold intensity dependence on the pulse width for various beam sizes for n-GaAs with a doping concentration of 7x10^{17} cm^{-3}. Note that the first term in Eq. (23) will be dominant for short exposure times where the damage threshold is primarily determined by the absorption depth (α_e^{-1}). Hence, the second term is dominant at long exposure times where the heat diffusion distance $(k\tau)^{1/2}$ is much greater than the absorption depth (α_e^{-1}).

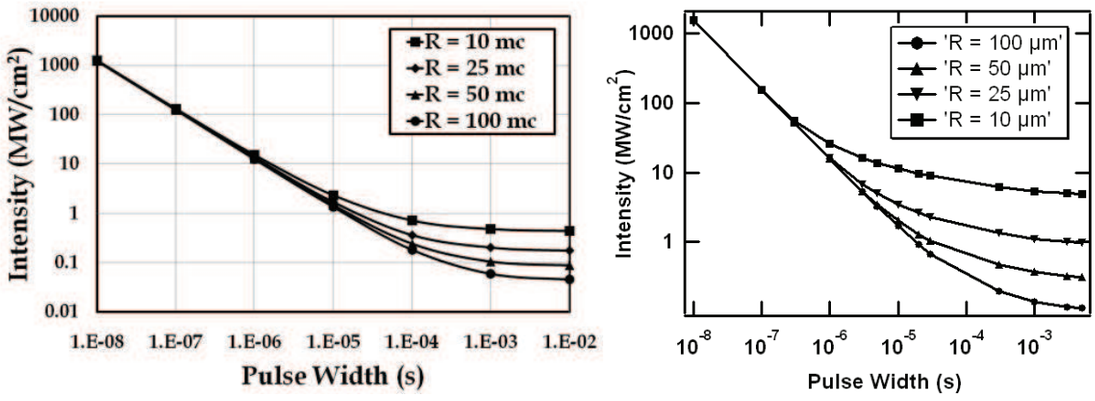

(a) (b)

Fig. 10. (a) Semi-infinite solid model based damage threshold intensity calculations for n-GaAs. (b) Finite solid model based damage threshold intensity calculations for n-GaAs (thickness 400 µm).

More accurate damage threshold intensities were calculated numerically by taken into account all relevant details of geometry and thermal configuration of the detector (n-GaAs substrate). Figure 10b illustrates the maximum allowable exposure time in function of the incident intensity for different pixel sizes. This figure was calculated for a 400 μm thick n-GaAs substrate with a doping concentration of $7x10^{17}$ cm^{-3}. The constraints on the curves are determined for a maximum lattice temperature increase of 500 K. Below 200 ns there is no more influence of the pixel size. This graph shows e.g. that for 10 μm radius pixels the maximum intensity of 10 μs pulses is 10 $MWcm^{-2}$.
Note that both models differs up to one order of magnitude at long exposure times. This can be attributed to the fact that the boundary conditions in terms of cooling efficiency play an important role at long exposure times for finite structures as the heat diffusion distance $(k\tau)^{1/2}$ becomes considerable with respect to the structure dimensions. For example, a pulse width of 10^{-2} s incident on a n-GaAs substrate results in a heat diffusion distance $(k\tau)^{1/2}$ of the order of 550 μm which is already larger than typical substrate thicknesses.
Bartoli et al. reported experimental damage threshold intensities of various IR detector materials. They show that intrinsic photodetectors (e.g. PbS, PbSe) have relatively low damage thresholds as compared to other IR detector materials due to their high absorption coefficient. Pyroelectric TGS damages at a much lower level than SBN or $LiTaO_3$ since the material is much more fragile and requires a smaller temperature increase for damage. HgCdTe, PbSnTe and InSb have comparable damage threshold intensities due to their similar material properties. Extrinsic photodetectors (e.g. Si:X, Ge:Y) are characterized by a high damage threshold as compared to other detector materials, primarily due to their low absorption coefficient. One can easily deduce for short exposure times, that the damage threshold intensity of a moderately doped (e.g. $7x10^{17}$ cm^{-3}) n-GaAs Seebeck detector is at least one order of magnitude higher than the threshold of HgCdTe based detectors.
The damage threshold of most thermal detectors can be fine-tuned by selecting the absorbing window material in function of the wavelength. Often a compromise will have to be made between detectivity and power handling capabilities.

3.6 Design possibilities

The main degrees of freedom that can be used in the design phase of a semiconductor based Seebeck detector are: the doping density, the doping layer thickness, the detector/pixel size, the type of electrode (finger contact or perimeter), and the implementation (single detector, four-quadrant position detectors, focal plane arrays).
As mentioned before, the type of detector output (intensity, energy or power) is determined by the ratio between the laser pulse FWHM and various time constants of the detector. Some of these time constants (e.g. τ_{ia}, τ_{mix}) are dependent on various design parameters, shown in expression 20 and 21, which can be tuned to extend a given regime of operation. For instance, the energy operation regime can be extended to longer pulse widths by increasing the absorption length and pixel size. Note that the absorption length can be increased in two ways: by increasing the highly doped absorption layer thickness for a thickness limited absorption length, or by decreasing the doping concentration (read absorption coefficient) for an absorption limited absorption length. This reasoning can be reversed for the extension of the power operation regime. Taken into account the doping level dependence of τ_{mix}, one can extend the energy regime towards shorter pulse widths by increasing the doping concentration.

The top electrode of the detector can be a finger contact (Figure 11a) which probes the local temperature in the neighborhood of the electrode or a perimeter design (Figure 11b) which measures the average temperature along the perimeter contact.

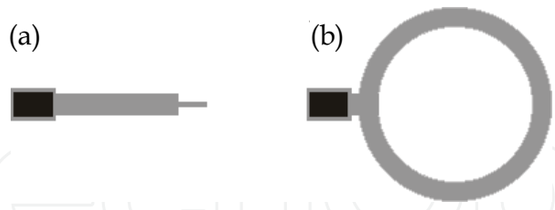

Fig. 11. (a) finger contact electrode; (b) perimeter contact electrode

Their design will determine the information one can get out of the detector. For pulse widths between τ_{mix} and τ_{ia}, the output of a finger contact electrode will be proportional to the local incident energy, whereas a perimeter contact, far from the heating center, allows to measure the total pulse energy incident within the perimeter of the detector. Note that energy measurements with a finger contact electrode allows, after post processing (differentiation), to obtain information about the temporal evolution of the local intensity. The total energy measurement obtained by use of the perimeter electrode on the contrary, allows, after differentiating the signal, to obtain information about the time evolution of the average intensity in the pixel. Special care should be taken in designing these electrodes in function of the pulse duration. Assuming a constant reference temperature, the detector's output will be proportional to the average potential on the contact area of the electrode. As it takes time to conduct heat through the substrate defined by the thermal diffusivity coefficient α_{th}, the electrode size should be carefully chosen in function of the pulse duration. The thermal diffusion length, which is dependent on the ratio between the pulse duration and the thermal time constant, can be taken as a measure (order of magnitude) for the maximum dimension of the contact electrode.

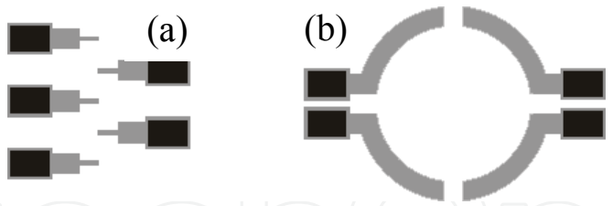

Fig. 12. (a) focal plane array detector; (b) four quadrant positioning detector

Seebeck based detectors can take many forms. In addition to the previously mentioned single pixel detectors, they can be implemented as a LFPA (e.g. for laser beam profilometry) or as a four quadrant positioning detectors as illustrated in figure 12a and 12b, respectively. Figure 13 shows a microscopic picture of a LFPA thermo-electric detector with squared perimeter contact pixels and a pixel pitch of 400 μm.

3.7 Thermal cross-talk

One of the major challenges regarding multi-pixel designs (e.g. laser beam profiler) are related to thermal cross-talk reduction. Thermal cross-talk can be defined as the unwanted signal measured by neighboring pixels as a consequence of thermal diffusion. Depending on the regime of operation, thermal cross-talk might be an important issue to cope with. This thermal cross-talk, which is mainly caused by heat transfer due to lattice vibrations can be

Fig. 13. LFPA thermo-electric detector with squared perimeter contact pixels

neglected in the intensity regime of operation, as there, the measured signal can be attributed to heated electrons. In the power regime on the other hand, the laser pulse width is long enough, with respect to the thermal time constant of the active material, to reach a thermal equilibrium between the input and output heat flux. Consequently, heat can diffuse inside the substrate resulting in a cross-talk signal in neighboring pixels. The penetration depth of heat inside the substrate can be approximated by (Ready, 1997)

$$D = \sqrt{4\alpha_{th} t_{FWHM}} \quad \text{with} \quad \alpha_{th} = \frac{k_{th}}{\rho C_p}$$

Where α_{th} is the thermal diffusivity, k_{th} is the thermal conductivity, ρ is the density, C_p is the volumetric heat capacity and t_{FWHM} is the pulse FWHM. For example, a Q-switched laser pulse of 100 ns incident on a GaAs based Seebeck detector results in a penetration depth of a few micrometers. The same detector reaches a thermal penetration depth of a few hundreds of micrometers for a one millisecond incident optical pulse. Hence, the thermal cross-talk level is strongly depend on the distance from the heating centre and the pulse duration. Hence, for linear focal plane arrays with a pixel pitch of a few hundred micrometers, this cross-talk level can be considerable for relatively long pulse widths (power operation regime).

It has been shown that the thermal cross-talk level can significantly be suppressed by applying a lock-in method (Vandermeiren et al., 2010). For lock-in periods significantly smaller than the thermal relaxation time, the thermal wave is strongly damped which limits it's propagation distance inside the substrate. Here, the optical pulse is amplitude-modulated (AM) as illustrated in figure 14 by means of a mechanical chopper or an external optical modulator (e.g. acousto-optic modulator).

The thermal diffusion length of the corresponding periodic heat source is then given by

$$\mu_{th} = \sqrt{\frac{\alpha_{th}}{\pi f_{Lock-in}}} \quad \text{with} \quad \alpha_{th} = \frac{k_{th}}{\rho C_p} \tag{25}$$

Where α_{th}, k_{th}, ρ, C_p and $f_{Lock\text{-}in}$ are the thermal diffusivity, thermal conductivity, density, volumetric heat capacity and modulation frequency, respectively. The thermal diffusion length dependence on the lock-in frequency is illustrated in figure 15a. The periodic

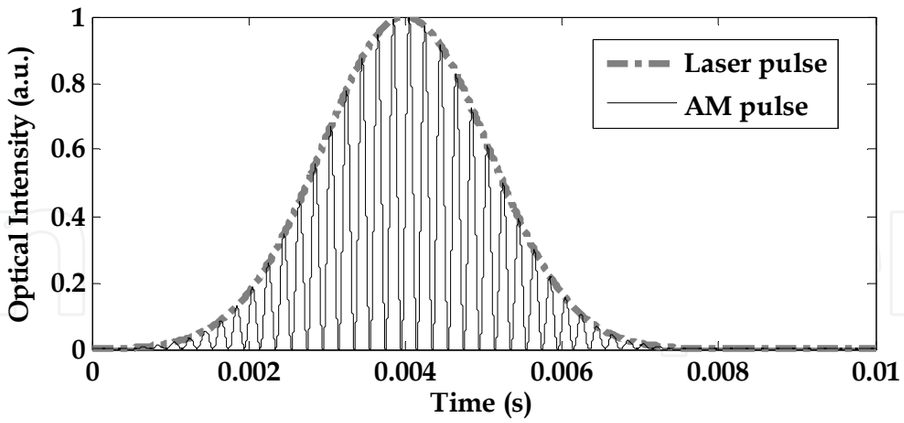

Fig. 14. Amplitude modulated laser pulse

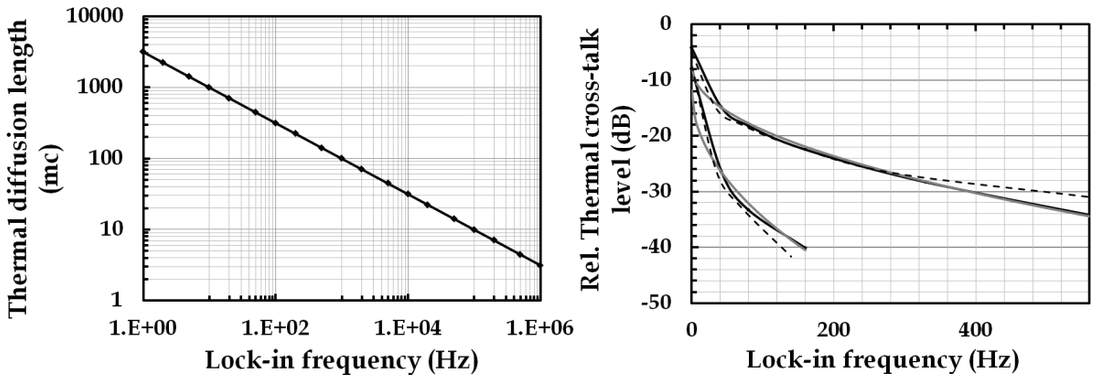

(a) (b)

Fig. 15. (a) frequency dependent thermal diffusion length; (b)Lock-in frequency dependence on the thermal cross-talk level

temperature increase at a distance r from the point-like heat source is described by Eq. (26) (Breitenstein & Langenkamp, 2003). Note that this equation only holds when the incident laser beam is small compared to the thermal diffusion length.

$$\partial T(r,t) = \frac{Q}{4\pi k_{th} r} e^{\left(-(1+i)\frac{r}{\mu_{th}}\right)} e^{i(2\pi f_{Lock-in})t} \tag{26}$$

Where Q, k_{th}, μ_{th}, r and t are the power, thermal conductivity, thermal diffusion length, the distance from the heat source and time, respectively. Hence, the periodic temperature increase for a fixed distance r is proportional to $\exp(-\sqrt{f_{Lock-in}})$.

By means of relation (26) one can analytically extract the cross-talk reduction factor for GaAs as a function of the modulation frequency and the distance from the heat source. The cross-talk reduction factor was numerically and experimentally quantified in previous work (Vandermeiren et al., 2010). The modulation frequency dependence on the thermal cross-talk reduction factor at a distance of 400 µm and 800 µm is shown in figure 15b. The

results of the analytical model (solid gray curves), a numerical finite element method (FEM) model (dashed gray curves) and experimental data (solid black curves) are in good agreement. For details about the numerical FEM model and experiments we refer to (Vandermeiren et al., 2010). Notice that the thermal cross-talk level can significantly be reduced by modulating the incident laser pulse. For example, in according with the analytical model, the cross-talk levels for the first and second adjacent pixels (r_{first} = 400 μm ; r_{second} = 800 μm), are attenuated by -10.5 dB and -19.3 dB respectively for a lock-in frequency of 140 Hz. The lock-in frequency should be chosen in function of the maximum allowable cross-talk level and the pixel pitch of a FPA-design. Expression 2 shows that the voltage responsivity of Seebeck detectors is inversely proportional to the lock-in frequency when $1 << \omega^2 r_{th}^2$. Figure 16 shows a measurement of the relative voltage responsivity dependence on the lock-in frequency for a n-GaAs based Seebeck detector. For lock-in frequencies exceeding about 400 Hz, the responsivity decreases with about 4 dB/kHz. The impact of this frequency dependent voltage responsivity reduction on the Johnson noise limited signal-to-noise ratio will be rather modest as the lock-in technique implies a narrow bandwidth as compared to a common broadband amplifier. This will significantly reduce the contribution of the Johnson noise which is approximately white.

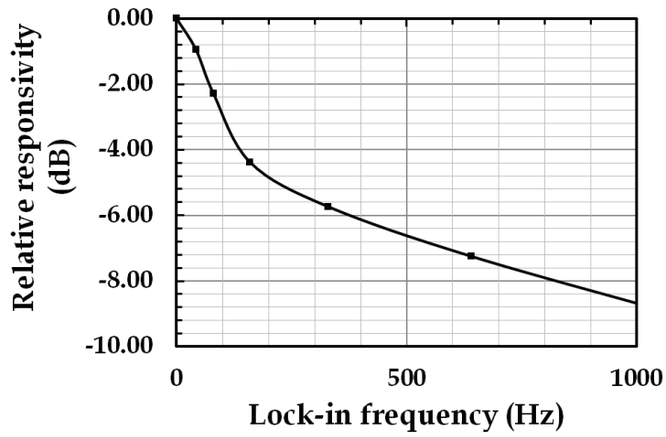

Fig. 16. Relative responsivity dependence on the lock-in frequency

3.7 Future directions of research

The ability of using thermo-electric LFPA for high power laser beam profilometry will be further investigated in the near future. A first aspect that will be considered when dealing with higher laser power levels is the impact of non-linear thermal effects on the thermo-voltage and thermal cross-talk level. These non-linearities include the temperature dependence of the absorption coefficient, the thermal conductivity, the Seebeck coefficient and the heat transfer coefficient. Furthermore, performance optimization in terms of electrical and thermal cross-talk, by improving the design and technology, will be tackled.

Another direction of research development will be dedicated to the implementation of high density 2D focal plane arrays. The main challenge here, in GaAs technology, is related to the implementation of multiplexing individual pixels to the electronics readout circuitry. Hence,

it might be worth to reconsider the material choice when dealing with 2D arrays. Silicon would be an obvious choice for implementing the readout electronics as one can benefit from standard CMOS technology. Hence, on the one hand we will investigate the ability of using silicon as the active detector material. However, on the other hand, we will consider the technological effort for using an arbitrary thermo-electric detector material stacked on a silicon die -comprising the readout electronics- by means of ball-bonding technology.

4. Conclusion

In this chapter we described, by means of introduction, most commonly used infrared detectors for measuring laser pulses used today with their respective advantages and disadvantages in terms of spectral detectivity, operation temperature and the damage threshold.

The theoretical background of semiconductor based Seebeck detectors was explained in detail. We showed that different operation regimes are applicable in function of the temporal characteristics of the optical input, due to various inherent time constants. These time constant permits to measure the intensity, energy or power in function of the incident pulse width. We also showed that the modelling and physical understanding of thermo-voltage detectors permits to optimize the detector design for a broad range of pulse parameters.

We showed that for most IR-detectors a trade-off exists between the responsivity and the power handling capabilities. We explained how one can control the responsivity and damage threshold of semiconductor based Seebeck detectors by means of the doping density and pixel geometry. It turns out that n-GaAs based Seebeck detectors with a moderate doping level ($7x10^{17}$ cm^{-3}) have a damage threshold which is about one order of magnitude higher than HgCdTe based detectors at short exposure times. This makes them suitable for short and intense pulse measurements.

We pointed out some design possibilities of Seebeck detectors in terms of functionality (single pixel, four quadrant or linear focal plane arrays) or the extension with respect to the pulse width interval of a particular regime of operation.

We showed quantitatively how one can improve the thermal cross-talk performance for LFPA's by means of a lock-in method. Hence, we demonstrated theoretically and experimentally that the thermal cross-talk amplitude can be reduced by -35 dB for the first neighboring pixel at a pixel pitch of 400 μm and at a lock-in frequency of 560 Hz. One can also conclude that the voltage responsivity reduction as a consequence of the lock-in frequency is small compared to the thermal cross-talk reduction. We expect the impact of the voltage responsivity reduction on the signal-to-noise ratio to be rather modest as the lock-in method implies that only a narrow bandwidth around the lock-in frequency can contribute to the noise level of the measured signal.

5. Acknowledgements

This work was funded by the Vrije Universiteit Brussel (VUB OZR1726, OZR1013BOF and GOA51/DEFIS42012-VUB) and the Brussels region in the context of the SOIB project (BRGEOZ128) on opto-electronic semiconductor components for CO_2 lasers.

6. References

Bartoli, F.; Esterowitz, L.; Kruer, M. & Allen, R. (1977). Irreversible laser damage in IR detector materials, *Applied Optics*, Vol. 16, 11, (November 1977), pp. 2934-2937, ISSN 0003-6935.

Breitenstein, O. & Langenkamp, M. (2003). *Lock-in thermography, basics and use for functional diagnostics of electronic components*, Springer-Verslag Berlin Heidelberg New York, ISBN 3 540 43439 9, Germany.

Blakemore, J. S. (1982). Semiconducting and other major properties of gallium arsenide. *J. Appl. Phys., Vol*. 53, 10, (October, 1982), pp. R123-R181, ISSN 0021-8979.

George, S.N.; Sharp, J. and Goldsmid, H.J. (2001) *Thermoelectrics: basic principles and new materials developments*, Springer-Verslag Berlin Heidelberg, ISBN 3-540-41245-x, Germany.

Phipps, C.R. (2007). *Laser Ablation and its Applications*, Springer Science, ISBN 0-387-30452-5, USA.

Razeghi, M. (1998). Current status and future trends of infrared detectors, *Opto-Electronics Review*, Vol. 6, 3, (September, 1998), pp. 155–194, ISSN 1230-3402.

Ready, J. F. (1997). *Industrial applications of lasers*, Academic Press, ISBN 0 12 583961 8, USA.

Rogalski, A. (2003). *Infrared Detectors: status and trends*, Progress in Quantum Electronics, Vol. 27, 2-3, pp. 59-210, (May 2003), ISSN 0079-6727.

Schubert, E. F. (1996). *Delta-doping of semiconductors*, Cambridge University Press, ISBN 0 521 48288 7, Great Britain.

Shah, J.; Leite, R.C.C. & Scott, J.F. (1970). Photoexcited hot LO phonons in GaAs, *Silid State Communications*, Vol. 8, 14, (May 1970), pp. 1089-1093, ISSN 0038-1098.

Shkerdin, G.; Stiens, J. & Vounckx, R. (1999). Comparative study of the intra- and intervalley contributions to the free-carrier induced optical nonlinearity in GaAs, *J. Appl. Phys*, Vol 87, 7, pp. 3807-3818, ISSN 0021-8979.

Shkerdin, G.; Stiens, J. & Vounckx, R. (2002) X-valley influence on hot free electron absorption and nonlinearities at 10.6 μm in highly doped GaAs, *European Phys. J. Appl. Phys,* Vol 19, 1, pp. 29-38, ISSN 1286-0042.

Shkerdin, G.; Stiens, J.; Kotov, V.; Vandermeiren, W. & Vounckx, R. (2007). Time dependence of CO_2 laser pulses recorded in the mixed detector regime of the photon drag and Seebeck effects in n-doped GaAs. *J. Appl. Phys.,* Vol. 102, 064509, (September, 2007), doi:10.1063/1.2779277, ISSN 0021-8979.

Stiens, J.; Shkerdin, G.; Vladimir, K.; Vandermeiren, W.; De Tandt, C.; Borghs, G. & Vounckx, R. (2006). Seebeck infrared photodetectors: an ultra wide dynamic range of design possibilities. *Proceedings of the SPIE,* pp. 61890, ISBN 0-8194-6245-4, Strasbourg, France, April 2006, SPIE-International Society for Optical Engineering, Bellingham, Washington.

Sze, S. M. (1981). *Physics of Semiconductor Devices 2nd edition*, John Wiley & sons, ISBN 0-471-05661-8, USA.

Vaissiere, J.C.; Nougier, J.P.; Fadel, M.; Hlou, L. & Kocevar, P. (1992) Numerical solution of coupled steady-state hot-phonon – hot-electron Boltzmann equation in InP,

Phys. Review B, Vol. 46, 20, (November 1992), pp. 13082-13099, ISSN 1098-0121.

Vandermeiren, W.; Stiens, J.; De Tandt, C.; Shkerdin, G.; Kotov, V.; Borghs, G.; Muys, P. & Vounckx, R. (2010). Thermal cross-talk reduction in IR thermo-electric photodetectors by lock-in method: 4D numerical simulations and experimental validation. *Proceedings of SPIE Photonics West – Physics and Simulation of Optoelectronic Devices XVIII*, pp. 75970Y-75970Y-9, ISBN 9780819479938, San Francisco USA, January 2010, SPIE-International Society for Optical Engineering, Bellingham, Washington.

Laser Pulse Phenomena and Applications
Edited by Dr. F. J. Duarte

ISBN 978-953-307-405-4
Hard cover, 474 pages
Publisher InTech
Published online 30, November, 2010
Published in print edition November, 2010

Pulsed lasers are available in the gas, liquid, and the solid state. These lasers are also enormously versatile in their output characteristics yielding emission from very large energy pulses to very high peak-power pulses. Pulsed lasers are equally versatile in their spectral characteristics. This volume includes an impressive array of current research on pulsed laser phenomena and applications. *Laser Pulse Phenomena and Applications* covers a wide range of topics from laser powered orbital launchers, and laser rocket engines, to laser-matter interactions, detector and sensor laser technology, laser ablation, and biological applications.

How to reference
In order to correctly reference this scholarly work, feel free to copy and paste the following:

Johan Stiens, Cathleen De Tandt, Gennady Shkerdin, Vladimir Kotov, Roger Vounckx and Werner Vandermeiren (2010). Infrared Thermo-Electric Photodetectors, Laser Pulse Phenomena and Applications, Dr. F. J. Duarte (Ed.), ISBN: 978-953-307-405-4, InTech, Available from: http://www.intechopen.com/books/laser-pulse-phenomena-and-applications/infrared-thermo-electric-photodetectors

INTECH
open science | open minds

InTech Europe
University Campus STeP Ri
Slavka Krautzeka 83/A
51000 Rijeka, Croatia
Phone: +385 (51) 770 447
Fax: +385 (51) 686 166
www.intechopen.com

InTech China
Unit 405, Office Block, Hotel Equatorial Shanghai
No.65, Yan An Road (West), Shanghai, 200040, China
中国上海市延安西路65号上海国际贵都大饭店办公楼405单元
Phone: +86-21-62489820
Fax: +86-21-62489821

IntechOpen